Transport of Gaseous Mixtures in a Porous Membrane Support Modelled Using a Random Three-Dimensional Pore Network

Čapek, P.
2013

Transport of gaseous mixtures in a porous membrane support modelled using a random three-dimensional pore network

P. Čapek, M. Veselý, [1]V. Hejtmánek
Institute of Chemical Technology, Technická 5, 166 28 Prague 6, Czech Republic,
Tel.: +420 220 444 407, e-mail: pavel.capek@vscht.cz; [1]Institute of Chemical Process Fundamentals of AS CR, Rozvojová 135, 165 02 Prague 6, Czech Republic

Introduction

Porous membrane supports and other porous media are in widespread use in many fields of chemical technology. The pore structure is inherently complex; therefore, many models of mass transport simply describe pore space as a continuum consistent with its appearance on a macroscopic scale (therefore a term *continuum models* is used [17]). Besides the pore space complexity, a number of fluid phases determine the nature of mass transport. Even when a relatively simple case of single-phase transport of gases is considered, a variety of mass transport mechanisms, including ordinary, Knudsen and surface diffusion, and viscous flow, can occur in pore space. All continuum models of mass transport involve empirical factors that describe transport characteristics of the pore structure. Note that a term *effective transport parameters of a porous solid* is used in the literature. The effective transport parameters, such as tortuosity, an effective pore radius, and an effective square of pore radii, have to be determined experimentally, usually from steady transport of inert gases. Unfortunately, this particular mass transport, which is hardly found in practice, only guarantees the parameter constancy. For example, it is known that tortuosity depends on the rate of chemical reaction [7,8].

On the other hand, random pore networks avoid the use of empirical factors and model the pore space as interconnected pores with random distribution of pore sizes. In addition, the pore networks naturally describe phenomena associated with multi-phase transport in pore space, e.g. existence of the percolation threshold [17]. For determination of pore space geometry and topology, several experimental methods have been developed for the past fifteen years, e.g. stochastic reconstruction [1,3,4,9–11,16,23,24] and X-ray computed microtomography [5,22].

The objective of this work is to demonstrate unusual phenomena that are inherent in transport of multi-component mixtures of ideal gases in porous solids. For this purpose, we simulated isobaric counter-current diffusion of binary and ternary gaseous mixtures in the porous membrane support represented by a pore network model. We also simulated non-isobaric transport of ternary mixtures in order to show the significance of small pressure gradients on overall mass transport.

1. Pore network models

A pore network was modelled as three-dimensional arrays of chambers connected by throats (chamber-and-throat network). The network consisted of throats with the constant rectangular cross-sectional shape (rectangular parallelepiped throats) and cubic or rectangular parallelepiped chambers. A chamber and three adjacent throats are depicted in Fig. 1.
Cubic or rectangular parallelepiped chambers were hierarchically arranged on nodes of two cubic arrays [2]. This specific arrangement of chambers enabled the construction of networks of relatively high total porosity ($\phi = 0.4292$) and a broad chamber size distribution (CSD). The procedure introduced a positive chamber-to-chamber (c–c) correlation in the pore network, i.e. large chambers were surrounded by chambers of similar sizes. An algorithm for the

efficient assignment of throat sizes to network bonds was implemented in such a way that we were able to introduce positive chamber-to-throat (c–t) correlation of a desired level. In this

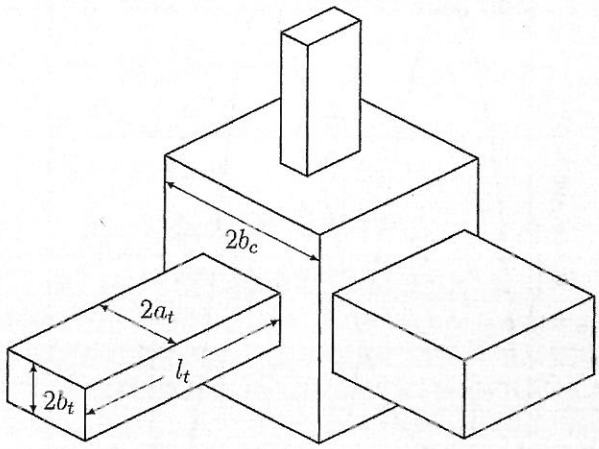

Figure 1: Schematic representation of a cubic chamber of volume $V_c = 8\,b_c^3$ and three adjacent rectangular parallelepiped throats. For throat sizes, a_t and b_t, the following inequalities hold: $a_t \le b_c$ and $b_t < b_c$ (an internal consistency limitation). The throat aspect ratio, $\lambda = a_t/b_t$, satisfies the inequality: $\lambda \ge 1$.

case of overlapping distributions, a certain level of c–t correlation was unavoidable regardless of the value of input parameters of the algorithm.

When a cubic network is to be of irregular topology, its mean coordination number, $\overline{Z}$, must be reduced by removing bonds at random. Then the coordination number, Z, of each chamber is equal to a random integer between 1 and 6. In this work $\overline{Z} = 4.0$ was estimated from a skeleton of reconstructed pore space. The chamber size and throat size (TSD) distributions (Fig. 2) were also derived from replicas of the α-alumina sample that was a subject of stochastic reconstruction [3]. The throat size distribution was modified using a procedure for iterative refinement of network parameters [2]. Having assigned chamber sizes to network nodes and throat sizes to network bonds, and having specified connectivity, the distance between the centres of gravity of two adjacent chambers was adjusted so that the total porosity, ϕ, of the network agreed with that of the prototype. Note that both chambers and throats contributed to the total pore volume. Further details of the network construction can be found elsewhere [2].

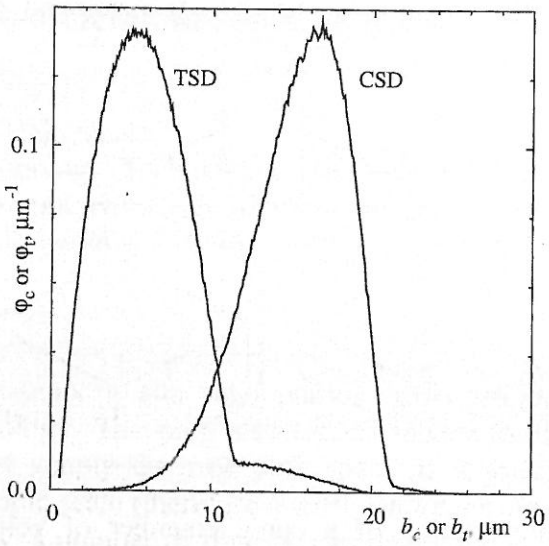

Figure 2: Number density functions of CSD, φ_c, and TSD, φ_t, used in the pore network.

2. Constitutive equations and mass balance in the pore network

Constitutive equations (models) based on the Maxwell-Stefan formulation accurately describe multi-component transport in pores. Four models of isothermal transport, involving Knudsen diffusion, ordinary diffusion and viscous flow, are in widespread use: the Dusty Gas Model [14], the Mean Transport Pore Model (MTPM) [18], the Binary Friction Model [12], and the Cylindrical Pore Interpolation Model [25]. The recent progress of transport phenomena theory and numerical methods enabled simulations of non-isothermal multi-component transport in porous media [6].

Schneider [18] originally derived the MTPM for isothermal multi-component transport of gases in long cylindrical capillaries. He considered both gradients of mole fractions (diffusion) and total pressure (forced flow) to evaluate fluxes of individual components, and also assumed that the contributions of diffusion and forced flow to the net flux of a component is in a first approximation independent and additive. For the purpose of pore-scale modelling, we restricted themselves to isothermal transport and adapted the MTPM and its transport coefficients to the special geometry of single pores of the pore network. A single pore schematically depicted in Fig. 3 consisted of a throat and the halves of adjacent chambers. Following Schneider's approach, we made a similar assumption that molar rates of diffusion and forced flow of individual components in non-cylindrical pores were independent and additive.

Our pore network calculations were further restricted to steady transport of inert gases, i.e. molar rates of diffusion and forced flow (not fluxes) were constant along the longitudinal axis of each single pore. Using this condition of steady state, we integrated constitutive equations taking into account the variable cross-section area of a single pore. Since driving forces of mass transport in a single pore were very small, the subsequent linearization of the integrated expressions in state variables, namely mole fractions and total pressure, was justified. Finally, molar rates of diffusion and forced flow of individual components as functions of the state variables located in centres of gravity of chambers (network nodes) were obtained.

Let $c^m_{[i]}$ and $c^m_{[j]}$ be the molar concentrations of the m-th gas in chambers (network nodes) i and j respectively. The molar rates, $\dot{n}^m_{[ij]}$, of flow between nodes i and j were obtained by solving a set of linear equations ($m = 1, ..., \mathrm{N_c}$)

$$\sum_{n=1}^{\mathrm{N_c}} \frac{\bar{c}_n \dot{n}^m_{[ij]} - \bar{c}_m \dot{n}^n_{[ij]}}{g^M_{ij}\, \bar{c}\, D^M_{mn}} + \frac{\dot{n}^m_{[ij]}}{g^K_{ij}\, w_m} + \alpha_m \sum_{n=1}^{\mathrm{N_c}} \frac{\dot{n}^n_{[ij]}}{g^K_{ij}\, w_m} = c^m_{[i]} - c^m_{[j]} \tag{1}$$

$$\alpha_m = \bar{c}_m \left(1 - \frac{\beta_m}{g^K_{ij}\, w_m} - \sum_{n=1}^{\mathrm{N_c}} \frac{\bar{c}_n \left(\beta_m - \beta_n\right)}{g^M_{ij}\, \bar{c}\, D^M_{mn}}\right) \left(\sum_{n=1}^{\mathrm{N_c}} \frac{\bar{c}_n\, \beta_n}{g^K_{ij}\, w_n}\right)^{-1}$$

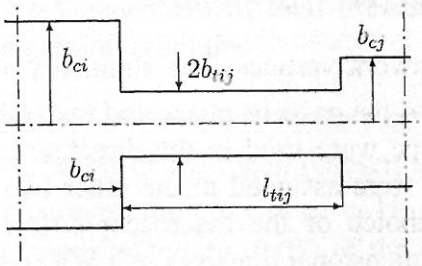

Figure 3: Scheme of a single pore consisted of a rectangular parallelepiped throat and the two halves of adjacent chambers.

where $\bar{c}_m = \left(c^m_{[i]} - c^m_{[j]}\right)/2$ is the mean value of the m-th molar concentration in a single pore, $\bar{c} = \sum_{m=1}^{\mathrm{N_c}} \bar{c}_m$ is the mean total molar concentration, D^M_{mn} is the bulk binary diffusion coefficient of the gas pair $m-n$, and w_m is the mean thermal velocity of molecules of gas m. Coefficients, β_m, related to permeability of a single pore depend on the mean molar concentrations, $\bar{c}_m$, due to a term consisting of mixture dynamic viscosity, μ, and the mean total molar concentration

$$\beta_m = g^K_{ij}\, w_n + g^V_{ij} \frac{RT\, \bar{c}}{\mu} \tag{2}$$

where R and T are the gas constant (8.314 J mol^{-1} K^{-1}) and the thermodynamic temperature, respectively.

For a single pore (cf. Fig. 3), conductance in the regime of molecular diffusion, g^M_{ij}, conductance in the Knudsen regime, g^K_{ij}, and viscous flow conductance, g^V_{ij}, were respectively given by

$$g^M_{ij} = 4 \left[\frac{1}{b_{ci}} + \frac{l_{tij}}{a_{tij} b_{tij}} + \frac{1}{b_{cj}}\right]^{-1} \tag{3}$$

$$g^K_{ij} = a_{tij} b_{tij} \left[1 - \frac{a_{tij} b_{tij}}{b_{ci} b_{cj}} + \frac{3\sqrt{\pi}\, l_{tij}}{16\sqrt{a_{tij} b_{tij}}}\right]^{-1} \tag{4}$$

$$g^V_{ij} = 16 \left[\frac{\xi(1)}{b^3_{ci}} + \frac{\xi\left(\lambda_{ij}\right) l_{tij}}{a_{tij} b^3_{tij}} + \frac{\xi(1)}{b^3_{cj}}\right]^{-1} \tag{5}$$

Perry et al. [15] gave a functional relationship between the shape factor, ξ, and the aspect ratio of rectangular ducts. We approximated their tabular data using a power expansion in $\lambda_{ij}^{-1} = b_{tij}/a_{tij}$

$$\xi(\lambda_{ij}) = 12 + 7.37043\,\lambda_{ij}^{-1} + 5.47478\,\lambda_{ij}^{-2} + 3.60699\,\lambda_{ij}^{-3} \tag{6}$$

To calculate molar rates of flow in individual single pores, mass balances for all network nodes had to be solved simultaneously. For simulation of steady network flow of inert gases, the molar rates, $\dot{n}_{[ij]}^{m}$, of flow that entered a network node had to be equal to the molar rates, $\dot{n}_{[jk]}^{m}$, leaving the node, i.e. mass had to be conserved

$$\sum_{i} \dot{n}_{[ij]}^{m} - \sum_{k} \dot{n}_{[jk]}^{m} = 0, \qquad j = 1, ..., N_V \tag{7}$$

where N_V is a number of network vertices. The simulated particle had the shape of a cube with two opposite sides open to the gaseous phase and remaining four sides closed. Boundary conditions of the Dirichlet type were used in the direction of macroscopic transport, while periodic boundary conditions were assumed in the other two principal directions. Since the network was isotropic, the choice of the macroscopic-flow direction was arbitrary. This arrangement resembled one-dimensional transport in a Wicke-Kallenbach cell, in which bases of a porous particle were rinsed by two gas streams of different composition [2]. The resulting system of non-linear equations (7) was solved using a damped Newton method, supplemented by an iterative solver (stabilised biconjugate gradient method) of the corresponding system of linear equations.

3. Results and discussion

In this section, simulations of transport of binary and ternary gaseous mixtures in pore networks are presented. All runs were performed on the same network with the only exception of the network size, N_V. Transport properties of gases and their mixtures were always evaluated at the constant temperature of 297 K. Molar rates, $\dot{n}_{[ij]}^{m}$, of flow in a plane perpendicular to a direction of macroscopic flow were summed and divided by an area of a cubic particle side. Resulting molar fluxes are presented as functions of the total pressure, P. Here, macroscopic flow was oriented along the x-principal direction.

3.1 Effect of network size

A pore network has to be sufficiently large to minimise finite size effects whilst making efficient use of computing time. The minimum network size ($N_V = 50 \times 50 \times 50$ nodes) above which simulations were almost free of network size effects was deduced from repeated constructions of networks of variable sizes and from network constructions with different seeds of random number generators. To ensure excellent statistical stability of results, we used the network size of $N_V = 100 \times 100 \times 100$ nodes as a reference case. This network corresponded to a cubic particle (particle side length, L = 4.4 mm), size of which was close to a real cylindrical pellet (height × diameter = 4.5 mm × 4.8 mm).

3.2 Effect of total pressure on isobaric diffusion

Transport of gases in porous solids is strongly dependent on total pressure. When a porous medium is given (i.e. pore size distribution is fixed), the total pressure determines the Knudsen number and the character of mass transport. A combination of narrow pores and low total pressure results in free-molecule transport, while wide pores and high total pressure imply ordinary diffusion and viscous flow. If there is no gradient of total pressure and if

transport of inert gases is only considered, the molar fluxes, J_m, must satisfy the Graham law generalised for the N_c-component mixture

$$\sum_{m=1}^{N_c} J_m \sqrt{M_m} = 0 \tag{8}$$

where M_m is the molar mass of a gas m. Transport of gases under the conditions that imply the validity of (8) is usually called counter-current isobaric diffusion.

Constitutive equations based on the Maxwell-Stefan theory, such as MTPM, are capable of predicting the smooth transition between free-molecule flow (Knudsen region) and continuum flow. Molar fluxes in the Knudsen region are proportional to total pressure, while molar fluxes at the continuum limit are independent of total pressure. In the following sections, isobaric diffusion in the transition region is studied.

3.2.1 Binary mixtures

The molar fluxes, J_1 and J_2, as functions of the total pressure, P, were simulated using counter-current isobaric diffusion of hydrogen (subscript $\equiv 1$) and nitrogen (subscript $\equiv 2$). In all simulation, runs the constant mole fractions of H_2 were assumed at the left-hand boundary (0.95) and at the right-hand boundary (0.05) of the particle. The results shown in Fig. 4 represent an example of "experimental" data that would enable very precise estimation of effective transport parameters of a porous solid, particularly tortuosity and the mean pore radius. The wide pressure interval in which the data were "measured" ensures that no transport mechanism prevails. Real experimental data, often found in the literature, are mea-

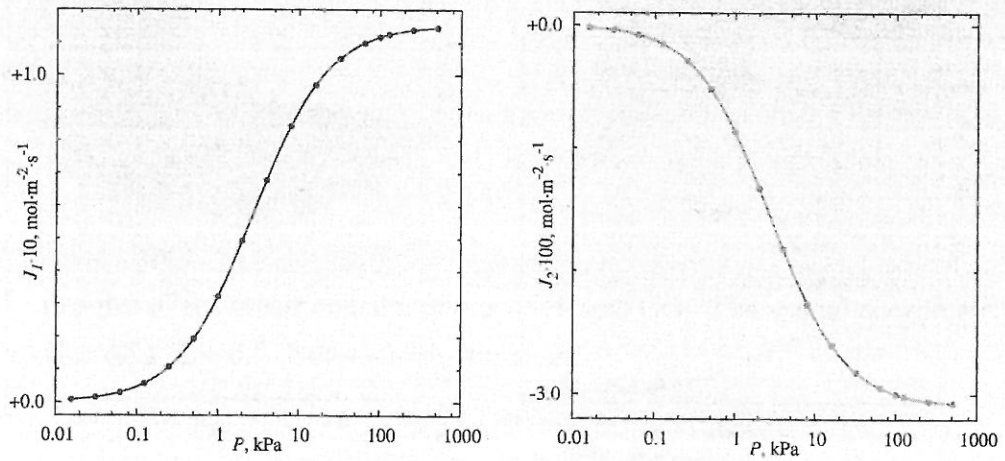

Figure 4: Molar fluxes of H_2 and N_2 as functions of the total pressure, P. Isobaric counter-current diffusion.

sured in a very narrow interval of total pressure, which can be a cause of some transport mechanism dominance and, therefore, of strong correlation between two estimated parameters [19–21].

3.2.2 Ternary mixtures

Transport in ternary or multi-component mixtures of ideal gases is surprisingly complex. The complexity stems from coupling of component fluxes. It is generally accepted that the Maxwell-Stefan formulation (e.g. MTPM given by eq. (1)) provides a very general approach for describing these unusual phenomena, and is superior to Fick's first law [13]. In order to demonstrate coupling of fluxes, we simulated counter-current isobaric diffusion in a ternary mixture of H_2 ($\equiv 1$), N_2 ($\equiv 2$) and CO_2 ($\equiv 3$), i.e. the gases were numbered in ascending order of their molar masses. The mole fractions of H_2, N_2 and CO_2 at the left-hand

particle boundary were respectively 0.49, 0.5 and 0.01, and the mole fractions of the same components at the right-hand particle boundary were respectively 0.01, 0.5 and 0.49, i.e. there was no Fickian driving force for diffusion of N_2. This choice of composition resembled Duncan and Toor's classical experiment, which was reviewed by Krishna and Wesselingh [13].

The courses of $J_1(P)$, $J_2(P)$ and $J_3(P)$ are depicted in Fig. 5. The positive flux of hydrogen indicated its diffusion from the left-hand boundary to the right-hand boundary. Carbon dioxide diffused in the direction opposite to that of hydrogen, i.e. both components behaved normally and moved down their respective composition gradients. When we examine $J_2(P)$, we see a curious phenomenon. In a low-pressure range, the molar flux of nitrogen was very small, conforming to transport in the Knudsen region. (Note that each component diffuses independently of others in the Knudsen region.) As the total pressure increased, the function $J_2(P)$ grew more steeply than the functions $J_1(P)$ and $J_3(P)$. For example, dividing their values calculated at the lowest and highest pressure, we obtained $J_1(512\,000)/J_1(15.625) \approx 103$, $J_3(512\,000)/J_3(15.625) \approx 103$ and $J_2(512\,000)/J_2(15.625) \approx$ ≈ 8940. It clearly showed that the course of $J_2(P)$ was strongly influenced by flux coupling. Nitrogen had the negative molar flux that was a result of frictional drags exerted by carbon dioxide and hydrogen on it. Obviously, the frictional drag of carbon dioxide was larger then that of hydrogen. However, the frictional drag of the heaviest component on a component of the middle molar mass need not be dominant. For example, counter-current isobaric diffusion

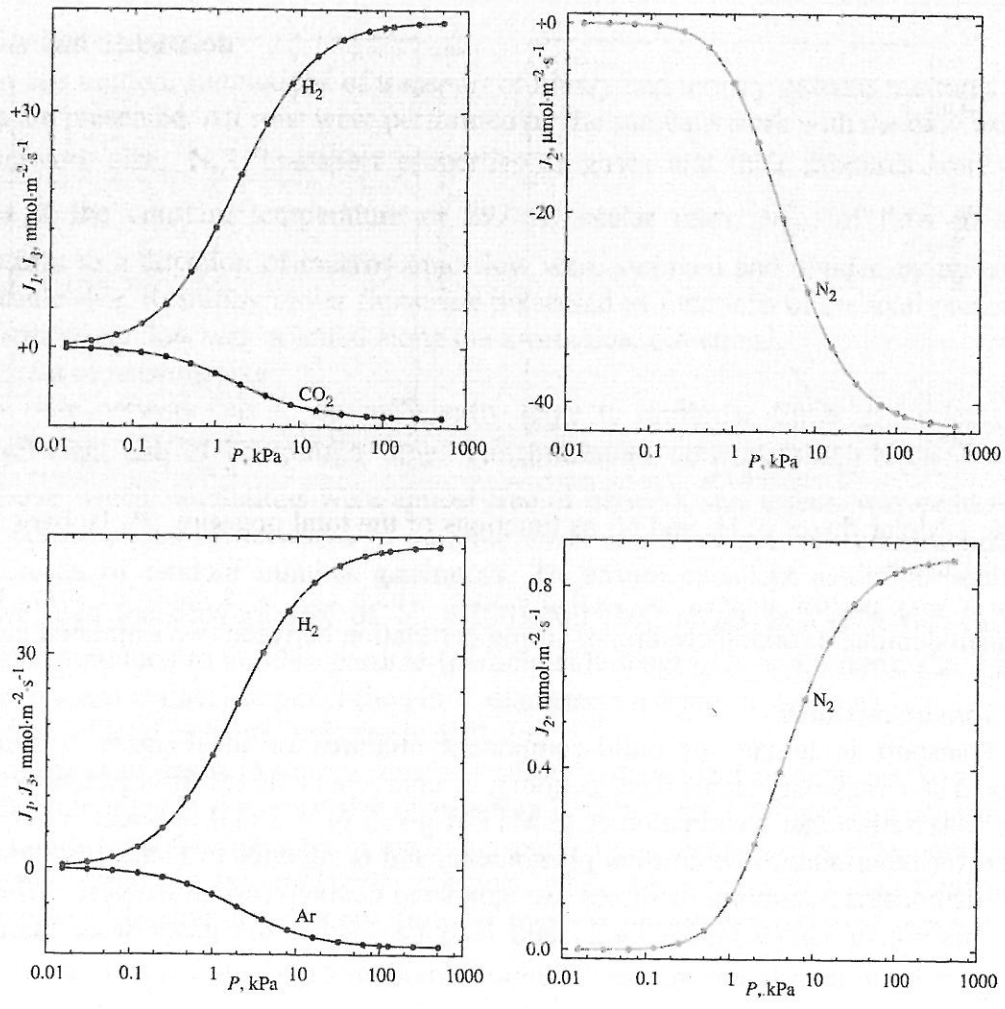

Figure 5 Molar fluxes, J_m, as functions of the total pressure, P. Isobaric counter-current diffusion. Top: H_2, N_2 and CO_2; bottom: H_2, N_2 and Ar.

in a ternary mixture of H_2, N_2, and Ar under the same conditions resulted in the positive molar flux of N_2, indicating the major role of the frictional drag exerted by hydrogen on nitrogen (cf. Fig. 5).

3.3 Effect of total pressure gradient on transport

The effect of the gradient of total pressure on transport in a ternary mixture of H_2, N_2, and CO_2 was also evaluated. The composition of gaseous mixtures at the particle boundaries was chosen to be the same as in section 3.2.2. However, the values of total pressure were respectively 100 kPa and 101 kPa at the left-hand boundary ($x = 0$) and at the right-hand boundary ($x = L$).

Concentration profiles of H_2, N_2, and CO_2 are shown in Figs. 6 and 7. The pressure difference of +1 kPa reversed the sign of J_1 (see Table 1) and forced hydrogen to move up its large con-

Table 1: Effect of the total pressure gradient on the molar fluxes of H_2 ($\equiv 1$), N_2 ($\equiv 2$), and CO_2 ($\equiv 3$).

ΔP, kPa	J_1, mol m^{-2} s^{-1}	J_2, mol m^{-2} s^{-1}	J_3, mol m^{-2} s^{-1}
0	$+4.078\times10^{-2}$	-4.093×10^{-5}	-8.694×10^{-3}
1	-5.615×10^{-3}	−0.2645	−0.2579

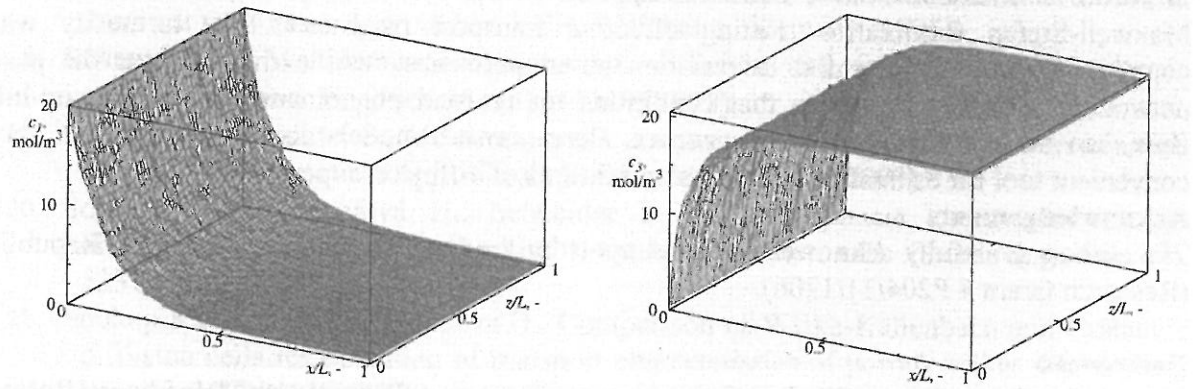

Figure 6 Profiles of the molar concentrations of H_2 and CO_2. The spatial coordinate, y, has a constant value of $y/L = 0.5$. Non-isobaric transport.

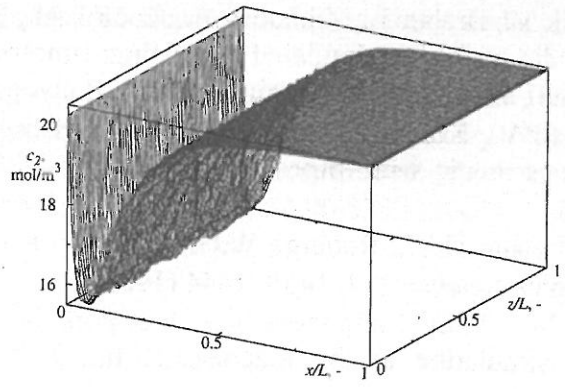

Figure 7 Profile of the molar concentration of N_2. The spatial coordinate, y, has a constant value of $y/L = 0.5$. Non-isobaric transport.

centration gradient (up-hill flow). The concentration profile and molar flux of CO_2 were fully consistent with the Fickian expectations, because carbon dioxide moved down its

macroscopic concentration gradient. While the concentration profiles of H_2 and CO_2 were normal, the profile of N_2 had a minimum in the direction of macroscopic flow. Since the molar flux of N_2 was negative, its flow could be termed normal (down-hill) between the x-coordinate of the minimum and the right-hand boundary. In the remaining part of the x-variable domain, however, up-hill flow of N_2 was observed.

The molar fluxes calculated for the isobaric and non-isobaric conditions are compared in Table 1. Absolute values of J_m implied that viscous flow prevailed in wide pores of the network. Its interaction with diffusion flow was the cause of the observed unusual phenomena, particularly up-hill flow.

The molar concentrations shown in Figs. 6 and 7 are not smooth functions of the spatial coordinates x, y and z. Microscopic fluctuations of state variables are a typical feature of pore network models of flow. They are also consistent with the discrete nature of porous media and irregular topology of their pore space. Pore network models contrast with continuum models of flow in porous solids. Continuum models neglect the influence of microscopic fluctuations of state variables on flow, i.e. state variables are smooth functions of the spatial coordinates.

4. Concluding remarks

In this paper, we developed a pore network model of multi-component mass transport in porous solids. Constitutive equations applied on the pore-scale level were based on the Maxwell-Stefan formulation. Fitting effective transport parameters like tortuosity was completely avoided. Essential information about pore sizes was extracted from the pore network model. It was shown that conditions for unusual phenomena, particularly up-hill flow, can be found quite often in practice. Pore network models also appear to be a very convenient tool for estimation of optimal conditions of diffusion experiments.

Acknowledgements

The authors gratefully acknowledge the support by the Grant Agency of the Czech Republic (Research Grant # P204/11/1206).

References

1. Adler P.M., *Porous Media: Geometry and Transport*. Butterworth/Heinemann, Boston (1992).
2. Čapek P., Hejtmánek V., Brabec L., Zikánová A., Kočiřík M., Effective diffusivity of gases in a reconstructed porous body. Chem. Eng. Res. Des., 86, 713–722 (2008).
3. Čapek P., Hejtmánek V., Brabec L., Zikánová A., Kočiřík M., Stochastic reconstruction of particulate media using a simulated annealing: Improving pore connectivity. Transp. Porous Med., 76, 179–198 (2009).
4. Čapek P., Hejtmánek V., Kolafa J., Brabec L., Transport properties of stochastically reconstructed porous media with improved pore connectivity. Transp. Porous Med., 88, 87–106 (2011).
5. Flannery B.P., Deckmann H.W., Roberge W.G., D'Amico K.L., Three dimensional x-ray microtomography. Science 237, 1439–1444 (1987).
6. Göll S., Piesche M., Multi-component gas transport in micro-porous domains: Multidimensional simulation at the macroscale. Int. J. Heat Mass Transfer, 55, 480–487 (2012).
7. Hollewand M.P., Gladden L.F., Modelling of diffusion and reaction in porous catalysts using random three-dimensional network model. Chem. Eng. Sci. 47, 1761–1770 (1992).

8. Hollewand M.P., Gladden L.F., Representation of porous catalysts using random pore network. Chem. Eng. Sci. 47, 2757–2762 (1992).
9. Jiao Y., Stillinger F.H., Torquato S., Modelling heterogeneous materials via two-point correlation functions. I. Basic principles. Phys. Rev. E, 76, 031110 (2007).
10. Jiao Y., Stillinger F.H., Torquato S., Modelling heterogeneous materials via two-point correlation functions. II. Algorithmic details and applications. Phys. Rev. E, 77, 031135 (2008).
11. Jiao Y., Stillinger F.H., Torquato S., A superior descriptor of random textures and its predictive capacity. Proc. Natl. Acad. Sci. U.S.A., 106, 17634–17639 (2009).
12. Kerkhof P.J.A.M., A modified Maxwell-Stefan model for transport through inert membranes: the binary friction model. Chem. Eng. J. 64, 319–343 (1996).
13. Krishna R., Wesselingh J.A., The Maxwell-Stefan approach to mass transfer. Chem. Eng. Sci. 52, 861–911 (1997).
14. Mason E.A., Malinauskas A.P., Evans III R.B., Flow and diffusion of gases in porous media. J. Chem. Phys. 46, 3199–3216 (1967).
15. Perry R.H., Green D.W., Maloney J.O., *Perry's Chemical engineers' handbook.* McGraw-Hill, New York, 6th edition, 1984.
16. Rozman M.G., Utz M., Efficient reconstruction of multiphase morphologies from correlation functions. Phys. Rev. E, 63, 066701 (2001).
17. Sahimi, M., *Flow and Transport in Porous Media and Fractured Rock: From Classical Methods to Modern Approaches*. VCH, Weinheim, Germany (1995).
18. Schneider P., Multicomponent isothermal diffusion and forced flow of gases in capillaries. Chem. Eng. Sci. 33, 1311–1319 (1978).
19. Šolcová O., Schneider P., Multicomponent counter-current gas diffusion: determination of transport parameters. Appl. Catal. A: General, 244, 1–9 (2003).
20. Šolcová O., Šnajdaufová H., Schneider P., Multicomponent counter-current gas diffusion in porous solids: the Graham's law diffusion cell. Chem. Eng. Sci., 56, 5231–5237 (2001).
21. Soukup K., Schneider P., Šolcová O., Comparison of Wicke-Kallenbach and Graham's diffusion cells for obtaining of transport characteristics of porous solids. Chem. Eng. Sci., 63, 1003–1011 (2008).
22. Spanne P., Thovert J.F., Jacquin C.J., Lindquist W.B., Jones K.W., Adler P.M., Synchrotron computed microtomography of porous media: Topology and transports. Phys. Rev. Lett. 73, 2001–2004 (1994).
23. Yeong C.L.Y., Torquato S., Reconstructing random media. Phys Rev. E 58, 495–506 (1998).
24. Yeong C.L.Y., Torquato S., Reconstructing random media II. Three-dimensional media from two-dimensional cuts. Phys Rev. E 58, 224–233 (1998).
25. Yong J.B., Todd B., Modelling of multicomponent gas flows in capillaries and porous solids. Int. J. Heat Mass Transfer, 48, 5338–5353 (2005).